Evaluation of defect formation in chalcopyrite compounds under Cu-poor conditions by advanced structural and vibrational analyses

Maxim Guc[1*], Eduard Bailo[2], Robert Fonoll-Rubio[1], Fabien Atlan[1], Marcel Placidi[1,6], Philip Jackson[3], Dimitrios Hariskos[3], Xavier Alcobe[4], Paul Pistor[5], Ignacio Becerril-Romero[1], Alejandro Perez-Rodriguez[1,7], Francisco Ramos[2], Victor Izquierdo-Roca[1*]

[1]*Catalonia Institute for Energy Research (IREC), Jardins de les Dones de Negre 1, 08930 Sant Adrià de Besòs, Spain*

[2]*Francisco Albero S.A.U. (FAE), Carrer Rafael Barradas, 08908, L'hospitalet de Llobregat, Barcelona, Spain*

[3]*Zentrum für Sonnenenergie- und Wasserstoff-Forschung Baden-Württemberg (ZSW), Meitnerstr. 1, 70563 Stuttgart, Germany*

[4]*Centres Científics i Tecnològics (CCiTUB), Universitat de Barcelona, C/ Lluis Solé i Sabaris 1-3, 08028 Barcelona, Spain*

[5]*Institute for Physics, Martin-Luther-Universität Halle-Wittenberg, Von-Danckelmann-Platz 3, 06120 Halle, Germany*

[6]*Departament d'Enginyeria Electrònica, Universitat Politècnica de Catalunya, C/ Jordi Girona 1, 08034 Barcelona, Spain*

[7]*Departament d'Enginyeria Electrònica i Biomèdica, IN[2]UB, Universitat de Barcelona, C/ Martí i Franqués 1, 08028 Barcelona, Spain*

**Corresponding authors: V.I.-R. (vizquierdo@irec.cat), M.G. (mguc@irec.cat)*

Abstract

Cu-poor compositions are key for obtaining high efficiency Cu(In,Ga)Se_2 (CIGSe) devices. These conditions lead to Cu deficit accommodation mechanisms like the formation of Cu-related defects

in the CIGSe crystal structure or of ordered vacancy compound. However, the origin of the benefits of Cu-poor compositions is still under discussion since these mechanisms are difficult to detect and characterize. In this work, a high precision Raman spectroscopy and X-ray diffraction analysis on a compositionally-graded CISe sample ([Cu]/[In] ratios from 0.48 to 1.03) allows us to shed light on this topic by reporting the detection of a "defective chalcopyrite phase" in the slightly Cu-poor compositional regime that may play a critical role, rather than other previously discussed mechanisms, on device performance. This phase is mainly characterized by the formation of a specific defect in the CISe structure which also contributes to appearance of a Raman peak at 230 cm^{-1}. Finally, the analysis of high efficiency (>18 %) CIGSe solar cells and the extrapolation of the results on defect formation obtained for CISe, suggest a possible impact of the defective chalcopyrite phase on the open circuit voltage of the devices, and opens a possible way to further investigate and develop the chalcopyrite based technologies.

Keywords: CIGSe, Raman spectroscopy, X-ray diffraction, Defects, Phase composition

1. Introduction

$Cu(In,Ga)Se_2$ (CIGSe) (and related compounds) is one of the most promising thin film photovoltaic (PV) technologies for the development of cost efficient solar cells. This is mainly related to its high absorption coefficient (>10^5 cm^{-1}) [1] and band gap tunability (from 1 to 1.7 eV by changing the In-Ga content) [2] that together with alkaline doping strategies [3,4] have led to a 23.35 % record solar cell at lab scale [5]. This constitutes the highest device efficiency achieved up to now for a thin film photovoltaic technology that has already reached the global PV market, and is comparable with the record efficiency of multi-crystalline Si [6], the dominant commercial technology. The control of Cu composition has been proved to be a key issue to achieve high efficiency devices. In particular, a Cu-deficient absorber surface has been observed to greatly enhance the open circuit voltage (V_{oc}) of CIGSe solar cells in comparison to purely stoichiometric absorbers [7]. Such a beneficial Cu-depleted surface is usually achieved using a 3-stage co-evaporation process (that also includes a Cu-rich intermediate process step for improving the crystalline quality of the layers) [8]. Additional device efficiency improvements have been recently achieved by the development of alkaline post deposition treatments (PDT) which, in turn, have also been linked to a reduction of Cu content at the absorber surface [3,9,10]. The efficiency

improvements observed in Cu-poor CIGSe devices are believed to be mainly due to a diminished recombination at the CdS/CIGSe interface [11,12].

Cu deficiency at the absorber surface is commonly accompanied by the presence of ordered vacancy compounds (OVC), i.e. $Cu(In,Ga)_3Se_5$ [13]. These compounds possess a wider bandgap than CIGSe and a band structure such that the conduction band alignment with CIGSe is rather flat while introducing a valence band offset that repels holes from the CdS/CIGSe interface which matches with the reduced recombination and improved device properties observed experimentally [14,15]. In fact, Nishimura et al. directly introduced $Cu(In,Ga)_3Se_5$ nanolayers at the CdS/CIGSe interface and obtained direct proof of this beneficial effect finding an optimum OVC thickness in terms of device performance [14]. Similarly, in a previous work, we showed a clear correlation between the relative contribution of a Raman peak attributed to an OVC vibrational mode with the V_{oc} of electrodeposited CIGSe solar cells allowing to define an optimum OVC content leading to the highest V_{oc} and photovoltaic efficiency [16].

All these previous results render clear that the analysis and profound comprehension of Cu-poor surfaces in CIGSe devices is of utmost importance to keep improving the technology. However, the exact mechanisms behind the beneficial effects of Cu-poor compositions are still under debate. As such, in this work, we present a thorough analysis of the influence of Cu-content on the structural properties of $CuInSe_2$ (CISe) and on the formation of the OVC phase for a wide range of compositions (with [Cu]/[In] ratios ranging between 0.48 and 1.03) by means of a detailed Raman scattering and X-ray diffraction analyses (XRD) of a compositionally-graded sample. The correlation between Raman and XRD measurements allows reporting the detection and evolution of a "defective chalcopyrite phase" in the slightly Cu-poor compositional regime (corresponding to [Cu]/[In] ratios between 0.7 and 1.0) that coexists with the OVC phase and plays a critical role, rather than other previously discussed mechanisms, on device performance. A detailed vibrational and structural characterization suggests that this defective chalcopyrite phase is the result of the formation of a specific defect in the CISe structure associated with the intensity enhancement of the Raman peak at 230 cm^{-1}. Finally, the analysis of high efficiency (> 18 %) CIGSe-based solar cells with slightly different [Cu]/([In]+[Ga]) content ratios, supposes a possible impact of the defective chalcopyrite phase on the open circuit voltage of the devices. The finding of this phase may represent a game change in the current understanding of chalcopyrite based PV devices, while

further investigations of it influence to the optoelectronic properties of the solar cells can be a possible way for the continues development of this technology.

2. Experimental details

The core of this work focuses on the study of a 10×10 cm^2 compositionally-graded $CuInSe_2$ (CISe) sample. The use of such graded sample enables the study of a wide compositional range within one sample in a practical way and ensures that all the sub-cells with different compositions analyzed in this work underwent the exact same fabrication process allowing to exclude process-related variations (a picture of the sample can be found at the left side of **Figure S1** of the Supporting Information). The compositionally graded sample was prepared on a Mo-coated soda-lime glass (SLG) substrate. In order to achieve a [Cu]/[In] compositional gradient, a spatially thickness-graded Cu layer was deposited on the substrate by DC-magnetron sputtering (Alliance AC450) with no holder rotation so that the grading occurred naturally as a consequence of the target-substrate geometry. An In layer was subsequently deposited onto it by thermal evaporation (Oerlikon Univex 250). In order to synthesize the $CuInSe_2$ phase, the Cu-In precursor was submitted to a thermal reactive annealing. It was first placed inside a graphite box together with elemental Se (100 mg, Alfa-Aesar, powder, 200 mesh, 99.999%). Then, the graphite box was introduced into a 3-zone tubular furnace where the following 2-step thermal annealing was performed: i) 400 ºC for 30 min at 1.5 mbar of Ar pressure (under continuous Ar flow); and ii) 550 ºC for 15 min at 1 bar of Ar pressure. A compositional mapping of the graded $CuInSe_2$ absorber sample was performed by X-ray fluorescence (XRF) using a Fisherscope XDV-SDD spectrometer. The measurements were carried out in a 100 (10×10) points grid covering the full area of the sample using a 50 kV accelerating voltage, a Ni10 filter to reduce the background signal and an integration time per measuring point of 45 s. As shown in **Figure S1** (right panel), a [Cu]/[In] compositional grading from ~0.5 to ~1.0 was obtained. These compositional data were used to select, identify and denote the areas measured in the subsequent XRD and Raman analyses. It should be noted that compositional variations due to different integrated area is reflected by different error values of XRF data in XRD and Raman analysis.

X-ray diffraction measurements were performed on selected areas covering the full compositional range by means of a PANalytical X'Pert PRO MPD alpha1 diffractometer in a Bragg-Brentano

θ/2θ configuration using Cu $K\alpha_1$ radiation (λ = 1.5406 Å), selected by means of a Johanson type Ge (111) focusing primary monochromator, and a X'Celerator silicon strip 1D detector. High resolution, high statistics, full angular range 2θ scans were obtained with the following parameters: 2θ/θ scans from 4 to 145º; step size 0.0166º; measuring time per step 200 seconds (X'Celerator active length 2.113º); 2 consecutive repeated scans; total measuring time per sample 7.5 hours. An automatic divergence slit system and a mask enabled a constant irradiated surface (10 × 12 mm^2) over the analyzed sample. It should be noted that, despite the relatively large irradiated surface, the compositional variations that exist within the surface area of a single XRD measurement can be neglected in comparison to the variations that exist between the different XRD measuring areas as can be deduced from the XRF mapping (**Figure S1**). The diffracting volume was constant over all the measured angular range taking into account the finite thickness of the analyzed thin film. Full profile analysis was performed with the TOPAS v6 software [17,18]. The background was modelled with a 15^{th} order Chebyschev polynomial. The instrumental contribution to the diffraction profile was calculated with the Fundamental Parameters Approach [19]. The width of the Bragg reflections for each phase was modelled with the Double-Voigt Approach [20] by considering both the Lorentzian contribution of the crystallite size effect and the Gaussian contribution of the microstrain to the reflections width.

Raman scattering spectra were measured on selected points covering the full compositional range (25 regions with dimensions 0.3×0.3 cm^2) using an *i*HR-320 monochromator from Horiba Jobin-Yvon coupled with a CCD detector. The measurements were performed in a backscattering configuration using an optical probe specifically designed at IREC (spot size diameter on the sample surface of ~70 μm). A solid-state laser with 785 nm laser line was used as excitation source with a laser power density of about 100 W/cm^2. These conditions ensured the absence of thermal effects in the Raman spectra. The spectra were calibrated by imposing the position of the main peak of monocrystalline Si to 520 cm^{-1}.

The structural characterisation of the CISe samples was further continued with Raman scattering and optoelectronic characterisation of high efficiency (>18 %) $Cu(In,Ga)Se_2$ (CIGSe)-based solar cells that were fabricated according to the processes described in [21]. The CIGSe absorbers were deposited on Mo-coated alkali-aluminosilicate glass substrates using a co-evaporation process. This was followed by a chemical bath deposition of a thin Zn(O,S) buffer layer, a sputtered (Zn,Mg)O and ZnO:Al window layer, and a Ni/Al grid. The final sample (1×5 cm^2) was

mechanically scribed into 10 solar cells with an area about 0.5 cm^2, and a slight variation of the compositional ratios was defined for each cell ([Cu]/([In]+[Ga]) = 0.91±0.02 and [Ga]/([In]+[Ga]) = 0.31±0.02) employing a similar XRF system to that described above. For the optoelectronic characterization of the solar cells, I-V measurements were made under illumination using a Sun 3000 class AAA solar simulator from Abet Technology. Measurements were carried out after the calibration of the system with a reference Si solar cell under AM 1.5 illumination and fixing the temperature of the samples to 298 K. The used excitation wavelength, 785 nm, allowed to perform the measurements directly on the complete devices and obtain signal only from the absorber without interaction with upper layers, due to their high band gap.

3. Results and discussions

Figure 1 shows the Raman spectra measured in the compositionally graded CISe sample in regions with different [Cu]/[In] ratios. The compositional gradient mainly results in the evolution of the relative intensity of the three bands centered at 153, 175 and 235 cm^{-1}. The peak at 175 cm^{-1} is associated to the A_1 symmetry mode of the chalcopyrite $CuInSe_2$ phase (related to Se-Se vibrations) [16,22], while the peaks at 153 and 235 cm^{-1} are associated to A_1 and B_2/E symmetry modes of the OVC phase [16]. For the region of the sample with the lowest Cu content ([Cu]/[In] = 0.48), the spectrum is in agreement with a pure OVC phase [23]. The increased intensity of the peak at 235 cm^{-1} is related to the existence of a quasi-resonant excitation of this vibrational mode under the 785 nm excitation wavelength employed, in accordance with previously reported results [16]. Increasing the [Cu]/[In] ratio decreases the relative intensity of the OVC peaks, and the main A_1 symmetry peak of the $CuInSe_2$ phase becomes the dominant one. In addition, a widening of the band close to 235 cm^{-1} is observed in the spectra with [Cu]/[In] ratios between 0.7 and 1.0. This widening is attributed to the enhancement of a peak located at 230 cm^{-1}, whose origin will be discussed later on.

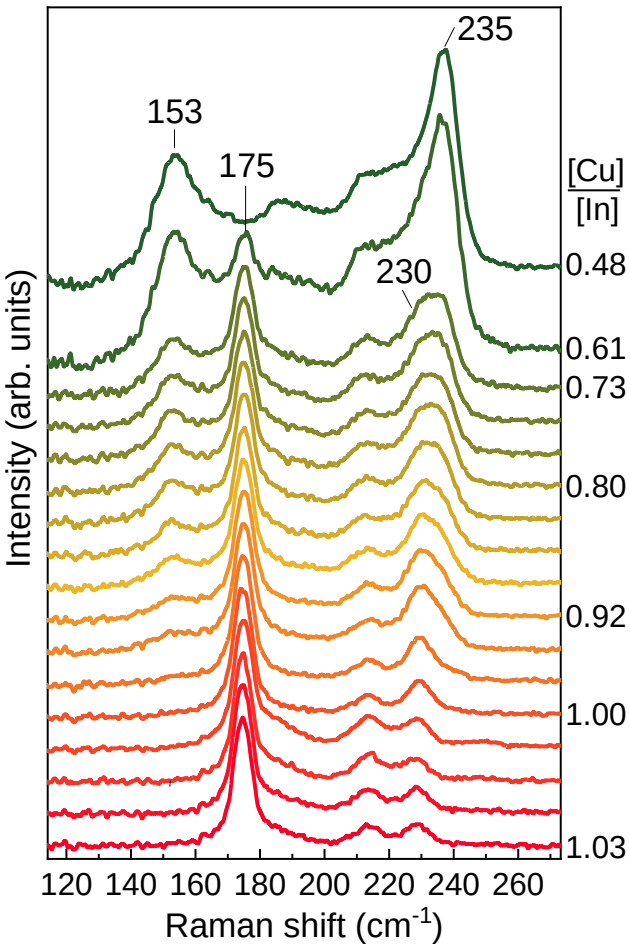

Figure 1. *Raman scattering spectra of different regions of the compositionally-graded CISe sample with different [Cu]/[In] ratios.*

In order to perform a detailed analysis of the evolution of the Raman spectra with the [Cu]/[In] ratio, the experimental spectra were fitted following the methodology proposed in Refs. [24,25] for the analysis of multiphase systems. This multiphase analysis methodology is based on the fitting of the experimental spectra employing linear combinations of the characteristic spectra of each expected component of the system (the reference spectra are normalized to the intensity of the highest peak). In the present case, the spectra measured experimentally at the regions of the sample with a [Cu]/[In] ratio 0.48 and 1.03 were used as references. The spectrum from the first region was attributed to pure OVC phase, as no traces of main CISe peak at 175 cm^{-1} were observed, and the spectrum from the second region was attributed to the pure or stoichiometric CISe (St-CISe) phase, as no evidences of secondary phases were found in it. As mentioned above, the fitting was made using linear combinations of the spectra of the pure phases (St-CISe and OVC

reference spectra) by selecting *A* and *B* coefficients until the minimum non-negative value of the residual parameter (R([Cu]/[In])) was reached, using the following equations:

$$I_{CISe}([Cu]/[In]) = A \times I_{CISe} + B \times I_{OVC} \quad (1)$$

$$R([Cu]/[In]) = I(x) - I_{CISe}([Cu]/[In]) \quad (2)$$

Here the I_{CISe}, I_{OVC} and I(x) correspond to the spectral intensities of the St-CISe, OVC reference spectra and spectral intensity of the experimentally measured spectrum of the specific region with x equal to the [Cu]/[In] ratio, respectively. The *A* and *B* are fitting coefficients related to the bound weight (between 0 and 1) of the St-CISe and OVC reference spectra, respectively.

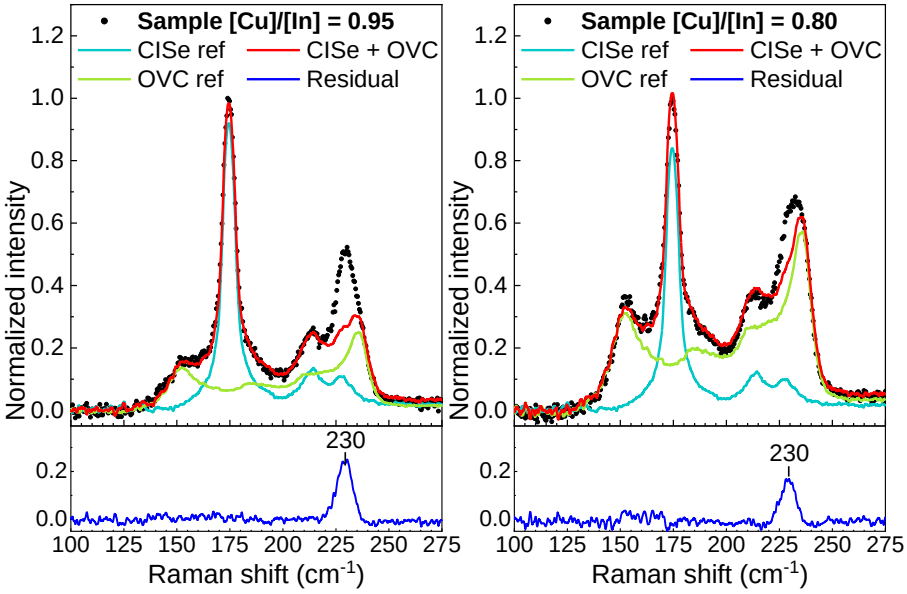

Figure 2. *Examples of experimental Raman spectra fitting employing linear combinations of the characteristic spectra of the St-CISe and OVC phases. The Residual (blue curve) is the difference between experimental (black dots) and overall calculated (red curve) spectra.*

Examples of the fitting results of the spectra from the slightly Cu-poor ([Cu]/[In] = 0.95) and Cu-poor ([Cu]/[In] = 0.80) regions of the compositionally graded sample are presented in the **Figure 2**. For most of the spectra measured in the regions with different [Cu]/[In] ratios the fitting shows good agreement between the measured and calculated spectra. However, for the regions with poor and slightly poor Cu content, a clear difference between the measured and calculated spectra is observed in the range close to 230 cm^{-1}. This discrepancy suggests the presence of an additional contribution to the Raman signal besides the reference OVC and St-CISe phases characterized by an unidentified peak at 230 cm^{-1}. The modelling of this peak allows to obtain a good fitting with a

Lorentzian curve with a full width at half maximum (FWHM) of about 8 cm^{-1}, which is comparable with the FWHM of the A_1 symmetry peak of the CISe phase (~7 cm^{-1}). Taking this into account, this additional peak was added to the Eq. (1), leading to a following expression:

$$I_{CISe}([Cu]/[In]) = A \times I_{CISe} + B \times I_{OVC} + C \times I_{230} \qquad (3)$$

In the Eq. (3), the newly added coefficient *C* is related to bound weight of the peak at 230 cm^{-1} and the I_{230} is the spectral dependence of this peak extracted from the residual spectra obtained as results of application of Eq. (1).

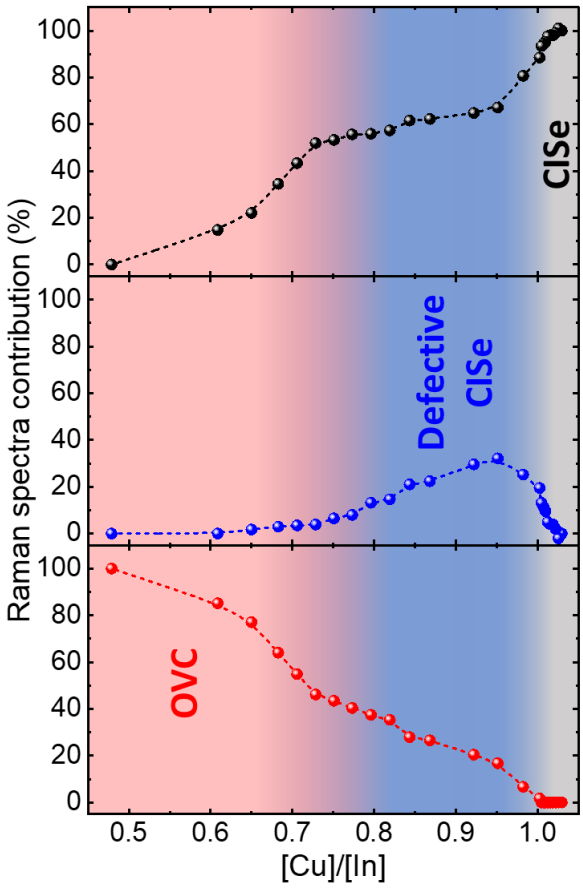

Figure 3. *A (top), B (bottom) and C (center) Raman fitting parameters (corresponding to the relative contribution of the St-CISe phase, the OVC phase and the 230 cm^{-1} peak in the Raman spectra (see Eq. (3)) versus the [Cu]/[In] content ratio. The dashed lines in all graphs are added as eye-guides for the reader and the regions with different colors correspond to different dominated phases. The errors in composition measurements due to the intrinsic inhomogeneities of the compositionally-graded CISe sample do not exceed the size of the data points.*

Appling Eq. (3) to the complete [Cu]/[In] ratio compositional range and normalizing the contribution coefficients *A*+*B*+*C* to 1, the evolution of the St-CISe, OVC and 230 cm^{-1} spectral

contributions can be extracted (see **Figure S2** for the fitting routine of the Raman spectra). **Figure 3** shows the relative contribution of these three components in function of the [Cu]/[In] ratio from which three main compositional regions can be observed and specified:

- [Cu]/[In] ≥ 1.00 (grey region): the St-CISe Raman contribution is the dominant one in the spectra and there is no contribution from the OVC phase;
- 0.75 ≤ [Cu]/[In] ≤ 1.00 (blue region): the St-CISe Raman contribution is still the dominant one in the spectra, but its relative intensity decreases gradually as [Cu]/[In] decreases. This is also accompanied by the appearance of the OVC contribution that increases gradually as the Cu content falls. Moreover, the peak at 230 cm^{-1} shows its maximum intensity in the 0.9 ≤ [Cu]/[In] ≤ 1.0 compositional region and has a strong decrease both for higher and lower [Cu]/[In] ratios;
- [Cu]/[In] ≤ 0.75 (red region): the OVC contribution becomes the dominant one in the Raman spectra and both the St-CISe and 230 cm^{-1} contributions decrease as the [Cu]/[In] content ratio decreases.

It is worth mentioning that the Raman signal is proportional to the concentration of the phase at sample surface. However, in order to carry out a quantitative analysis, a calibration of the phase content with the Raman signal should be first performed, which is outside of the scope of the present study. Nevertheless, the evolution of the phase content shown in this work is independent of such calibration. Additionally, the Raman spectra of the compositionally-graded CISe sample were measured under 632.2 and 532 nm excitation wavelengths. Examples of fitting by linear combination of reference spectra (**Figure S3** and **S4**) and detailed results description are presented in the Supporting Information.

From the dependencies presented in **Figure 3**, it can be observed that the decrease of the St-CISe contribution with the decreasing Cu content has two sharp slopes: the first one is related to the fast increase of the 230 cm^{-1} peak contribution (in the range 0.95 ≤ [Cu]/[In] ≤ 1.00) and the second one is related to the fast increase of the OVC phase contribution ([Cu]/[In] ≤ 0.7). These results suggest two different mechanisms of Cu-deficit accommodation in the crystalline lattice of the CISe compound: the first one dominates in a very Cu-poor content ([Cu]/[In] ≤ 0.7) and is related to formation of the OVC phase, and the second dominates in the slightly Cu-poor range (0.75 ≤ [Cu]/[In] ≤ 1.00) and is related to the newly found contribution at 230 cm^{-1}. It is interesting to remark that the latter range includes the compositional region typically employed for the

fabrication of high efficiency $CuInSe_2$ and $Cu(In,Ga)Se_2$ solar cells [3,21,26,27]. Moreover, it is necessary to specify that the compositional limits of appearance and/or domination of specific phases indicated in the present study might be slightly varying depending on the absorber deposition technology, formation path, post-deposition treatment and other technological processes that may have a significant effect on defect formation.

Regarding the origin of the observed enhancement of the intensity of the peak at 230 cm^{-1}, it does not agree with a possible appearance of vibrational modes related to elemental Se, Cu_xSe or In_xSe secondary phases since the compounds from these systems have their main Raman peaks quite far from the 230 cm^{-1} spectral region (see e.g. [28-30] for the Cu_xSe phases, [31-35] for In_xSe and [36] for elemental Se). In addition, the FWHM of the peak is comparable to that of the other peaks present in the spectra, which allows excluding the possibility of the 230 cm^{-1} peak being related to a low crystalline quality or amorphous phase. Thus, it seems highly unlikely that the increased intensity observed for the 230 cm^{-1} peak is related to the presence of any additional secondary phase. In view of these observations, we believe that the 230 cm^{-1} peak should be interpreted as related to the activation or enhancement of a chalcopyrite CISe vibrational mode as a consequence of the Cu-poor structural defects that appear in the compositional region [Cu]/[In] $\leq$ 1.00. This could be related either to the activation of the $E/B_{1/2}$ symmetry modes out of the Γ-point (center of Brillouin zone) [37] or to the enhancement of one of the E/B_2 symmetry modes at the Γ-point which have been experimentally found to be close to the 230 cm^{-1} position [22,38]. According to the calculated phonon density of states [37], the peaks above 210 cm^{-1} are mainly related to mutual vibrations of In-Se chain, which allows to assign the peak at 230 cm^{-1} also to this type of vibrations. The appearance of a new peak (or enhancement of an existing one) suggests that a CISe defective phase, which is slightly different from the St-CISe chalcopyrite phase formed under the stoichiometric conditions, is formed in the Cu-poor compositional region. It is important to notice that the proposed CISe defective phase is characterized by the presence of the same peaks than the St-CISe phase, but with a higher intensity of the peak at 230 cm^{-1} as the only difference. This similarity makes complicated to detect the coexistence of the defective and stoichiometric CISe phases in the Cu-poor compositional range by Raman spectroscopy. On the other hand, the decrease of the 230 cm^{-1} contribution for [Cu]/[In] $\leq$ 0.75 might be related to a significant contribution of the peaks of the OVC phase rather than to the retrieval of the CISe stoichiometric structure. This was further investigated by means of XRD analysis.

In previous works, the accommodation of defects related to the Cu deficit in the Cu-In-Se system was correlated with the formation of the OVC phase observed by Raman and XRD studies [15,23]. However, slightly Cu-poor samples are barely studied and the influence and effect of Cu deficit on defect formation is discussed only in a limited amount of samples from this compositional range or in a limited compositional range [39,40]. In order to shed light on this topic and complement the Raman spectroscopy analysis presented above, high resolution XRD measurements were performed in regions of the compositionally graded CISe sample with [Cu]/[In] ratios ranging from 1.03 to 0.51 as described in the *Experimental details* section. The diffractograms obtained are presented in **Figure 4** for relevant angular ranges while examples of full diffractograms are presented in **Figure S5**. The analysis of the XRD data shows the existence of the CISe compound with a tetragonal chalcopyrite type structure (space group $I\bar{4}2d$) in all the analyzed regions. In regions with $0.94 \leq$ [Cu]/[In] ≤ 1.03, this $I\bar{4}2d$ chalcopyrite is the only phase observed. Below [Cu]/[In] = 0.76, a mixture of the chalcopyrite phase with a $CuIn_3Se_5$ OVC phase that presents a tetragonal stannite type structure (space group $I\bar{4}2m$) can be observed. Although the diffraction patterns of the CISe chalcopyrite type phase and the OVC stannite type phase are very similar (most of the reflections are nearly at the same positions and show very similar relative intensities) the high resolution wide angular range XRD data allows their clear distinction. This is possible since the position of the reflections at close diffracting angles slightly changes due to small differences in the cell parameters and, mainly, due to the fact that the hhl reflections with (2h + l) $\neq$ 4n are forbidden by the *d* glide plane of the $I\bar{4}2d$ structure and allowed in the $I\bar{4}2m$ structure (in practice, the main additional reflections observed in this $I\bar{4}2m$ OVC phase are the 002, 110, 114, 222 and 118 at 2θ values close to 15.4º, 21.8º, 38.2º, 47.3º and 69.1º, respectively). Furthermore, all the XRD diffractograms show the presence of the Mo back contact and of a highly oriented $MoSe_2$ phase.

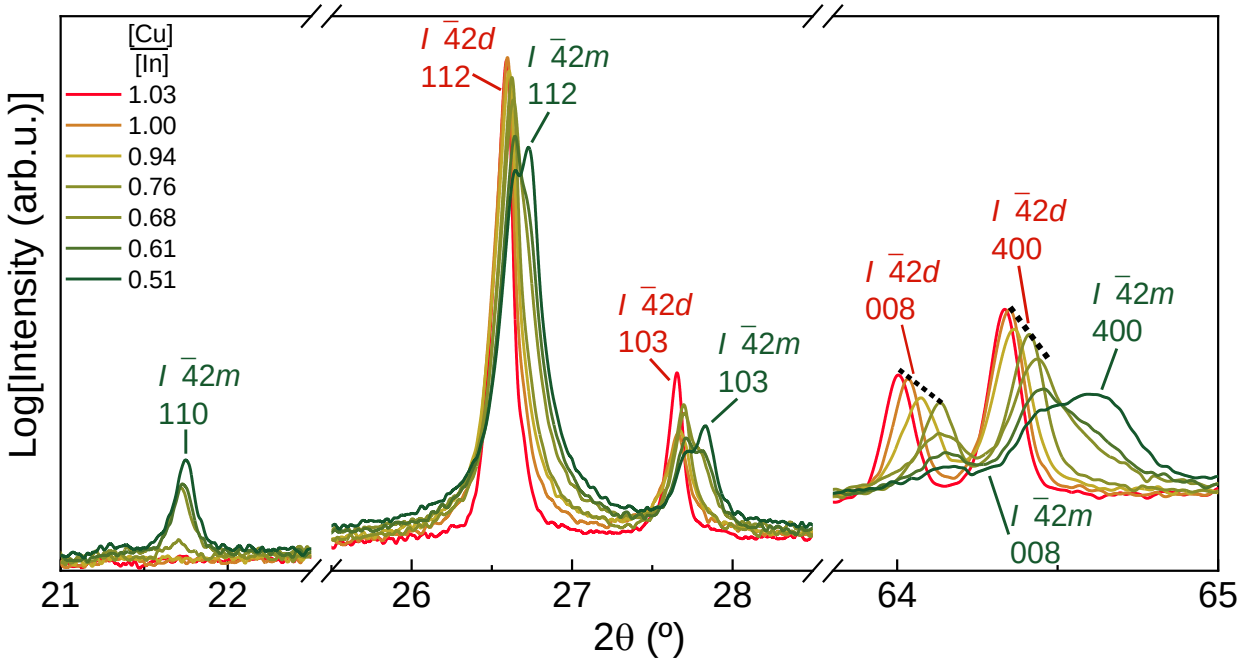

Figure 4. *XRD diffractograms of the CISe samples with different [Cu]/[In] content ratios.*

In order to characterize the structure and microstructure of the phases observed by XRD, and to check the validity of the conclusions extracted from the Raman-based phase analysis involving the potential presence of a defective CISe phase in the Cu-poor compositional regime, a full profile analysis of the CISe chalcopyrite phase and the OVC stannite phase was performed by Rietveld refinement [41]. The Mo and $MoSe_2$ Bragg reflections were fitted independently and were not constrained to their structures. The starting structural models for the CISe and OVC phases are taken respectively from Refs. [42] and [43]. In the case of the CISe chalcopyrite structure, atomic substitutions of Cu by In in the 4b (0,0,1/2) Wyckoff position was enabled by refining their corresponding occupation factors. In the case of the OVC $CuIn_3Se_5$ stannite structure, the atomic coordinates, the occupation factors, and the temperature factors were fixed to their starting values, so only the scale factor, the cell parameters, and the microstructural parameters were refined. Excellent refinements were obtained for all measurements and detailed information of the analysis can be found in the supplementary information: **Table S1** reports the agreement factors, cell parameters, estimated crystallite size and microstrain, and the semi-quantitative content of the CISe and OVC phases; **Table S2** shows the site occupation factors in the chalcopyrite phase; and **Figure S6** depicts the Rietveld plots of representative measurements in samples with [Cu]/[In]

ratios 1.02, 0.94 and 0.51. The main findings from the Rietveld refinement analysis (also shown in **Figure 5**) can be summarized as follows:

- There are no reflections broadening of the chalcopyrite CISe phase for [Cu]/[In] ratios from 1.03 to 1.01. The *c* cell parameter and, thus, the cell volume slightly decrease with the decreasing Cu content (**Figure 5a**). Both Cu and In cations are in their original Wyckoff positions (**Table S2**).
- For [Cu]/[In] ratios of 1.00 and 0.94, similarly to the range above, a good refinement is obtained with chalcopyrite CISe as the only phase. However, clear reflections broadening is observed which becomes more evident as the Cu content decreases. This is related to the decrease of average estimated crystallite size (from 860 to 370 nm (**Figure 5b**)) and to the detected microstrain (**Table S1**). The cell parameters clearly decrease with the decreasing Cu content: from a cell volume of 389 $Å^3$ for [Cu]/[In] > 1, to a cell volume of 388.8 $Å^3$ and 388.4 $Å^3$ for [Cu]/[In] = 1.00 and [Cu]/[In] = 0.94, respectively. Furthermore, the calculated site occupation factors show the presence of small amounts of In in Cu position and Cu in In position. The shrinkage of the cell, the microstructure broadening and cation position interchange matches with a defective CISe phase for these stoichiometric and slightly copper deficient compositional regions.
- For the more Cu-deficient measuring areas ([Cu]/[In] ratios from 0.76 to 0.51), the mixture of a CISe chalcopyrite $I\bar{4}2d$ phase and an OVC stannite $I\bar{4}2m$ phase detected by Raman is confirmed. The CISe phase also shows cell shrinkage (**Figure 5a**) and similar microstructure reflections broadening as for Cu-richer compositions (**Figure 4**) that increases with the decreasing Cu content. The cell volume ranges from 387.6 to 386.9 $Å^3$ and the estimated crystallite size from ~400 to ~200 nm (**Figure 5b**) with estimated microstrain δd/d values of around 0.0003. The site occupation factors indicate the presence of defects related to Cu and In cation substitutions, and only a slight decrease of the amount of Cu atoms in In position is observed with the decreasing [Cu]/[In] ratio (**Table S2**). The OVC phase also shows reflections broadening that seems approximately constant over the different measured areas and that, if caused by microstructure, would have an estimated crystallite size of around 100 nm and a δd/d microstrain of around 0.0005. The semi-quantification results of the OVC phase content in the regions with [Cu]/[In] ratios equal to 0.76, 0.68, 0.61 and 0.51 were found to be around 9, 26, 40 and 61 %, respectively.

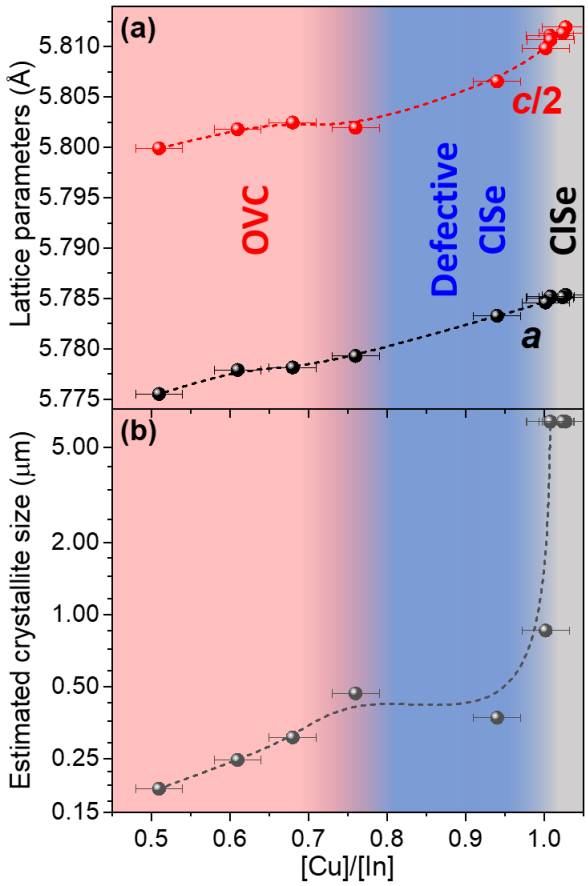

Figure 5. *(a) Dependence of the lattice parameters of the chalcopyrite phase on the [Cu]/[In] ratio. (b) Evolution of the crystallite size versus the [Cu]/[In] ratio. The dashed lines in both graphs are added as eye-guides for the reader and the regions with different colors correspond to different dominated phases.*

These XRD data confirm the observations made by Raman analysis with a dominant CISe phase at high [Cu]/[In] content ratios and a dominant OVC phase at low [Cu]/[In] content ratios. In addition, the analysis of the XRD diffractograms also confirms the existence of a transition region that is characterized by a relevant reduction of the chalcopyrite lattice parameters (**Figure 5a**), together with a strong decrease of the estimated crystallite size (**Figure 5b**), and with change of the site occupation factors of both Cu and In cations (**Table S2**). These features confirm the formation of a transition phase at the compositional region [Cu]/[In] ≤ 1.0, which we have named "defective chalcopyrite phase" and which is characterized by a high density of structural defects. It is worth noticing that the mentioned defective chalcopyrite phase cannot be strictly considered as a new phase of the chalcopyrite compounds since it presents just minor differences compared to the standard stoichiometric chalcopyrite phase (mainly related to the increased amount of point

defects that leads to the observed decrease of lattice parameters and of crystallite size) while maintaining the same crystalline structure with the space group $I\bar{4}2d$ (see Figure 6). In the present study, the notation "defective chalcopyrite phase" is used mainly for convenience to refer to the changes that occur in St-CISe phase and to show their possible role for high efficiency devices, as will be discussed later on. Based on the refinement results of the diffractogram measured from the region with [Cu]/[In] = 0.94, a crystalline structure model of the defective chalcopyrite phase is proposed and is shown graphically in **Figure 6** together with the crystalline structures of the St-CISe and OVC phases [44]. Here, the main difference of the defective chalcopyrite structure model from the stoichiometric St-CISe and from the OVC phases is mainly exhibited by the presence and/or type of the point defects at the 4a Wyckoff position: only Cu ions are at this position in St-CISe; together with Cu ions, both V_{Cu} and In_{Cu} defects are slightly probable in defective CISe; together with Cu ions, only the V_{Cu} defect appears at this position in OVC with a quite high probability.

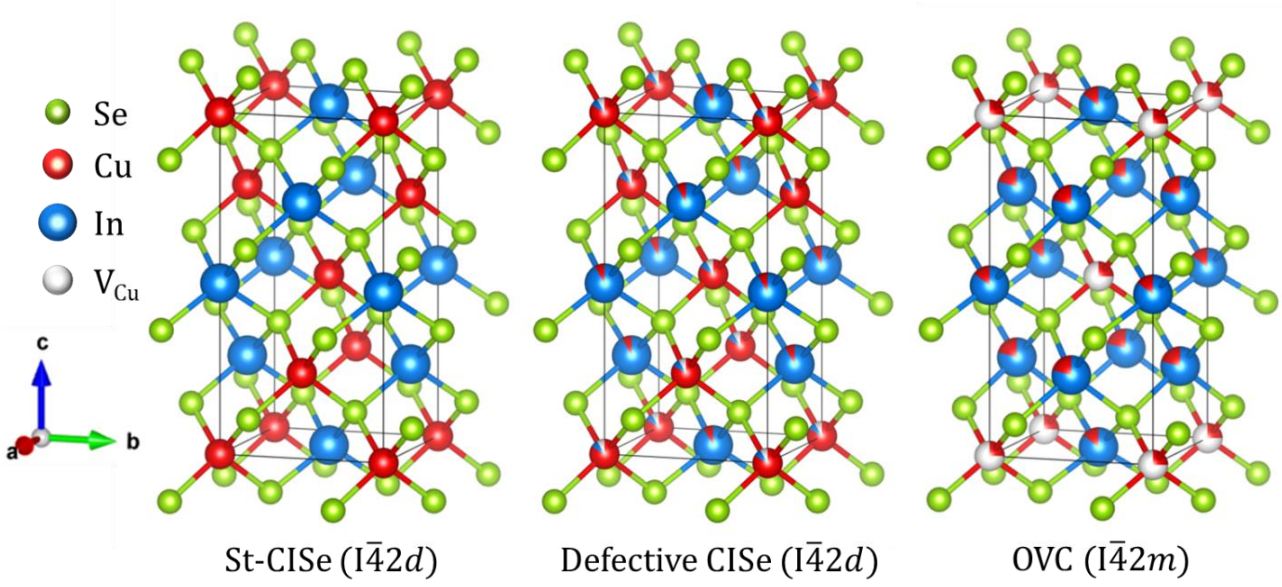

Figure 6. *Crystalline structure models of stoichiometric (St-CISe) and defective (Defective CISe) chalcopyrite phases together with the OVC phase. Drawings produced by VESTA program [44].*

The formation of a defective phase in Cu-poor conditions strongly supports the assignment of the 230 cm^{-1} Raman contribution in this compositional region to a defect-activated chalcopyrite vibrational mode. Regarding the possible defects involved in this defective chalcopyrite structure, *ab-initio* calculations show that in Cu-poor In-rich p-type CISe the point defects with the lowest formation energy are V_{Cu} and In_{Cu}, which also participate in the formation of the electrically neutral

cluster defect $[2V_{Cu}^{-} + In_{Cu}^{2+}]$ [45]. Similar defects and increase of their concentration with the decrease of the Cu content were also found by the neutron diffraction analysis of the CISe compound [40]. Our previous considerations about the involvement of In cations vibrations in the 230 cm^{-1} Raman peak and the presence of a measurable amount of In atoms at the Cu position deduced from XRD analysis are in accordance with the proposed crystalline structure model, indicating that this peak is mainly related to the presence of In_{Cu} point defects or of $[2V_{Cu}^{-} + In_{Cu}^{2+}]$ cluster defects in the crystal lattice. Previously, the influence of the changes in chemical composition, or the deviation from stoichiometry, on the relative intensity of Raman peaks was observed in cubic Cu_2SnS_3 [46] and in tetragonal $Cu_2ZnSnSe_4$ compounds [47,48]. In the former compound, the effect was explained by the changes in the S environment due to alloying with the Cu_3SnS_4 phase. However, changes in defect concentration due to the changes in the cationic ratio (discussed in Ref. [46]), can affect in a similar way the S environment. In the case of the kesterite type $Cu_2ZnSnSe_4$ compound (which can be seen as structurally evolved from the chalcopyrite compounds [49]) the change in the concentration of different point and/or cluster defects was shown to result in changes in the intensity of the specific Raman peaks that are assigned to vibrations of the ions involved in the formation of such defects. For instance, the change in intensity of the peaks in the high wavenumber range (above the main Raman peak of $Cu_2ZnSnSe_4$) was correlated to the change of the concentration of substitutional Zn_{Sn} defects [47,48]. These, together with the isovalency and similarities in crystal structure of CISe and $Cu_2ZnSnSe_4$ compounds supports the supposition expounded above about the change in intensity of the peak at 230 cm^{-1} being related to changes in the concentration of In_{Cu} substitutional defects.

Finally, in order to evaluate the possible impact of these defects on the device performance, a detailed Raman scattering analysis of high efficiency $Cu(In,Ga)Se_2$ (CIGSe) solar cells was performed (see spectra in the **Figure S7**). The devices were fabricated following the processes described in [21] with slight variations of the [Cu]/([Ga]+[In]) (CGI = 0.89 – 0.92) and [Ga]/([In]+[Ga]) (GGI = 0.30 – 0.33) compositional ratios and efficiencies ranging between 18.0 and 20.8 % (see **Table S3** in the Supporting Information for more details). CISe and CIGSe are structurally equivalent compounds and present similar vibrational properties which makes the transfer of the results obtained in CISe to the CIGSe material plausible. Indeed, the partial substitution of In cations by Ga leads to a small decrease of the lattice parameters and, as consequence, to the shortening of the bond length and to the energy increase of the optical phonons

ultimately shifting the Raman peaks to the higher wavenumbers [50-52]. Thus the contribution of the defect induced peak in the CIGSe compound is shifted from 230 cm^{-1} to the 235 – 245 cm^{-1} spectral region. Due to the absence of reference spectra of the chalcopyrite and OVC phases with a certain Ga content, the detailed multiphase analysis could not be performed in the CIGSe sample. In order to overcome this issue, a simpler methodology was applied. This is based on the calculation of the relative integrated intensity of the peaks in the spectral range where the defect related peak is expected (235 – 255 cm^{-1} in the case of CIGSe compound). The intensity of this defect induced Raman peak was found to have strong correlation with the CGI ratio and with the open circuit voltage (V_{oc}) of the devices. **Figure 7** shows the V_{oc} versus the integrated intensity ratio of the defect induced Raman peak and the main CIGSe Raman peak. As it can be seen in this figure, the V_{oc} increases and tends to saturate in a maximum value around 715 mV when the relative contribution of the defect induced Raman peak related to a defective chalcopyrite structure increases. This agrees with the behavior previously reported in [16], where we observed the existence of an optimum value of the relative intensity of this Raman contribution leading to solar cells with highest V_{oc} and device efficiency when analyzing electrodeposited $Cu(In,Ga)Se_2$ solar cells (efficiencies in the 13 – 15 % range). In this previous work, though, this peak was tentatively attributed to a vibrational mode from the OVC phase. Yet, the detailed structural analysis reported in the present work allows us to reassign this peak to the defect induced Raman mode characteristic of a defective chalcopyrite CISe phase present in Cu-poor absorber layers.

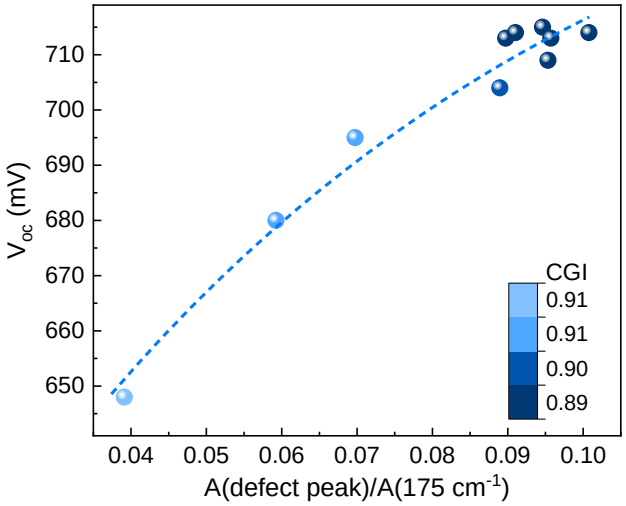

Figure 7. *Open circuit voltage of CIGSe based solar cells versus relative contribution of the defect induced Raman peak. The color scale represents [Cu]/([Ga]+[In]) (CGI) ratio in each cell.*

It should be noted that in addition to the change of CGI ratio in the analyzed high efficiency solar cells, the GGI ratio was also slightly varied (see **Table S3**), which cannot be completely excluded as an additional factor influencing the V_{oc} of the devices. However, a comparison of the V_{oc} with the measured GGI ratio do not exhibits any clear correlations between this two parameters, e.g. an almost constant V_{oc} is observed for the cells 1 to 7, for which the GGI was changed from the minimum to maximum values (**Table S3**). In this regard, from the results obtained in the present study it can be concluded that, even though its nature is still not perfectly clear, the defective chalcopyrite phase can play a critical role on device performance as proved by the evident correlation of the intensity of the Raman peak related to this phase with the V_{oc} of the devices. This correlation suggests that this defective phase has mainly importance at the absorber/buffer interface and/or in the space charge region, since mainly the absorber surface is assessed by Raman spectroscopy under the used excitation conditions (the 785 nm excitation wavelength is expected to penetrate ~100 nm in the absorber layer). It is also worth mentioning that in the compositionally-graded CISe sample the XRD analyses do not show coexistence of the defective and stoichiometric chalcopyrite phases, meaning that the former is distributed throughout the bulk of the sample. However, the higher simplicity of the fabrication process of this sample does not lead to any in-depth elemental gradient contrarily to the case of the CIGSe absorber employed in high efficiency devices. The latter might present an associated more complicated in-depth distribution of defects and the presence of the defective chalcopyrite phase can vary in the bulk and the interfaces of the absorber layer, which can be a challenge for future studies. Nevertheless, the found coexistence of the defective chalcopyrite phase with the OVC phase at the absorber surface of high efficiency solar cells (see **Figure S7**), raises in turn questions about the importance of OVC in the device performance. Long time disputes about the positive effects of a Cu-depleted surface in chalcopyrites resulted in the generally accepted assumption that the superficial OVC phase plays a critical role in the device efficiency improvement due to its wider band gap that has a beneficial effect on band alignment by effectively suppressing interface recombination [13,45,53,54]. On the other hand, further experimental evidences led to the conclusion that only the very top of the absorber layer is strongly Cu-depleted [55,56], and that, in general, there are no hard crystallographic evidences of the presence of a phase distinct from the OVC phase in absorber grade chalcopyrites. More recently, as stated in the *Introduction* section, an important efficiency boost of chalcopyrite photovoltaic devices was achieved by employing heavy alkali post

deposition treatments at the absorber surface. Although, the nature of the positive effect of such treatments is still not clear, indications of a pronounced Cu-depletion at the CIGSe surface as a result of the post deposition treatment were found [3,56], together with a reduction of the OVC phase content [57]. This might be indicating that the role of the OVC phase at the absorber surface has been overestimated and that, in reality, this phase simply coexists with the more beneficial defective chalcopyrite phase found in the present study which is also formed under Cu-poor conditions. Despite the mentioned ambiguities in the nature and beneficial role of the different phases of Cu-In(Ga)-Se system that may be present at the absorber/buffer interface due to Cu-depletion, the present work shows a clear correlation of device performance with the intensity of the Raman peak related to the defective chalcopyrite phase. As such, we strongly believe that the results presented in this work demonstrate that this defective chalcopyrite phase, which had remained under the radar until now (at least from the technological point of view), may play a fundamental role in the high efficiencies achieved by the CIGSe PV technology, and it further development can be related with a more profound understanding of possible role of this novel phase to the device performance. In addition, this work confirms the potential of Raman scattering spectroscopy as an advanced characterization technique for the assessment of the opto-electronically relevant modifications at the absorber/buffer interface. This is even more important as compositional variations of the absorbers are lately playing a crucial role for the different alkali surface treatments in highest efficiency devices. It indicates that, through further research and development, Raman spectroscopy can play a pivotal role in process/device development and might be employed as a fast and non-destructive methodology for device quality control and efficiency prediction within fabrication lines at the very early stages of the production process.

4. Conclusions

In conclusion, a thorough and detailed structural analysis of a compositionally-graded $CuInSe_2$ (CISe) chalcopyrite sample synthesized with a wide range chemical compositions (including very Cu-poor and slightly Cu-rich compositions) has been performed combining Raman spectroscopy and XRD. This analysis has allowed to identify the presence of a compositional region (corresponding to [Cu]/[In] content ratios between 0.7 and 1.0) that is characterized by the coexistence of a defective $CuInSe_2$ chalcopyrite phase and an OVC phase. This has been possible

thanks to a detailed fitting of the Raman spectra using a multiphase analysis methodology that has revealed for the first time the presence of a defect-activated chalcopyrite vibrational mode located at 230 cm^{-1} related to the defective CISe phase. This defective chalcopyrite-OVC phase coexistence has been corroborated by a detailed high precision XRD study including Rietveld refinement analyses. Finally, the combination of Raman spectroscopy with optoelectronic characterization has revealed the existence of a possible correlation between the relative contribution of the defect-activated peak in the Raman spectra related to the defective chalcopyrite phase and the open circuit voltage of high efficiency (> 18 %) CIGSe photovoltaic devices. This suggests that this defective phase may play a critical role, rather than other previously discussed mechanisms, on device performance, which however should be further investigated.

Acknowledgements

M.P., X.A. and A.P.-R. acknowledge financial support from the Spanish "Agencia Estatal de Investigación" under the WINCOST project (ENE2016-80788-C5-1-R). E.B. acknowledges financial support from Doctorat Industrial program (ACCIO-Generalitat de Catalunya). Authors from ZSW are grateful for the Federal Ministry for Economic Affairs and Energy support within the project CISHiTec (contract No 0324179). Authors from IREC and the University of Barcelona belong to the SEMS (Solar Energy Materials and Systems) Consolidated Research Group of the "Generalitat de Catalunya" (Ref. 2017 SGR 862), and acknowledge the financial support of Solar-Era.Net project DURACIS (Spanish subproject Nr. PCIN-2017-041). M.P. and M.G. acknowledge the financial support from Spanish Ministry of Science, Innovation and Universities within the Ramón y Cajal (RYC-2017-23758) and Juan de la Cierva (IJC2018-038199-I) programs, respectively.

References

[1] K.L. Chopra, P.D. Paulson, V. Dutta, Thin-film solar cells: an overview, Prog. Photovoltaics 12 (2004) 69–92. https://doi.org/10.1002/pip.541

[2] B.J. Stanbery, Copper indium selenides and related materials for photovoltaic devices, critical reviews in solid state and materials sciences, Crit. Rev. Solid State 27 (2002) 73–117. https://doi.org/10.1080/20014091104215

[3] A. Chirilă, P. Reinhard, F. Pianezzi, P. Bloesch, A.R. Uhl, C. Fella, L. Kranz, D. Keller, C. Gretener, H. Hagendorfer, D. Jaeger, R. Erni, S. Nishiwaki, S. Buecheler, A.N. Tiwari, Potassium-induced surface modification of Cu(In,Ga)Se_2 thin films for high-efficiency solar cells, Nat. Mater. 12 (2013) 1107–1111. https://doi.org/10.1038/nmat3789

[4] D. Hauschild, D. Kreikemeyer-Lorenzo, P. Jackson, T.M. Friedlmeier, D. Hariskos, F. Reinert, M. Powalla, C. Heske, L. Weinhardt, Impact of a RbF postdeposition treatment on the electronic structure of the CdS/Cu(In,Ga)Se_2 heterojunction in high-efficiency thin-film solar cells, ACS Energy Lett. 2 (2017) 2383–2387. https://doi.org/10.1021/acsenergylett.7b00720

[5] Solar Frontier Press Release "Solar Frontier Achieves World Record Thin-Film Solar Cell Efficiency of 23.35%" (2019). http://www.solar-frontier.com/eng/news/2019/0117_press.html (accessed April 16, 2021).

[6] News releases "Canadian solar sets a 23.81% conversion efficiency world record for n-type large area multi-crystalline silicon solar cell" (2020). https://investors.canadiansolar.com/news-releases/news-release-details/canadian-solar-sets-2381-conversion-efficiency-world-record-n (accessed April 16, 2021).

[7] S. Siebentritt, L. Gütay, D. Regesch, Y. Aida, V. Deprédurand, Why do we make Cu(In,Ga)Se_2 solar cells non-stoichiometric?, Sol. Energy Mater. Sol. Cells 119 (2013) 18–25. https://doi.org/10.1016/j.solmat.2013.04.014

[8] A.M. Gabor, J.R. Tuttle, D.S. Albin, M.A. Contreras, R. Noufi, A.M. Hermann, High-efficiency $CuIn_xGa_{1-x}Se_2$ solar cells made from $(In_x,Ga_{1-x})_2Se_3$ precursor films, Appl. Phys. Lett. 65 (1994) 198–200. https://doi.org/10.1063/1.112670

[9] A. Laemmle, R. Wuerz, M. Powalla, Investigation of the effect of potassium on Cu(In,Ga)Se_2 layers and solar cells, Thin Solid Films 582 (2015) 27–30. https://doi.org/10.1016/j.tsf.2014.10.088

[10] F. Pianezzi, P. Reinhard, A. Chirilă, B. Bissig, S. Nishiwaki, S. Buecheler, A.N. Tiwari, Unveiling the effects of post-deposition treatment with different alkaline elements on the electronic properties of CIGS thin film solar cells, Phys. Chem. Chem. Phys. 16 (2014) 8843–8853. https://doi.org/10.1039/c4cp00614c

[11] M. Turcu, O. Pakma, U. Rau, Interdependence of absorber composition and recombination mechanism in Cu(In,Ga)$(Se,S)_2$ heterojunction solar cells, Appl. Phys. Lett. 80 (2002) 2598–2600. https://doi.org/10.1063/1.1467621

[12] D. Regesch, L. Gütay, J.K. Larsen, V. Deprédurand, D. Tanaka, Y. Aida, S. Siebentritt, Degradation and passivation of $CuInSe_2$, Appl. Phys. Lett. 101 (2012) 112108. https://doi.org/10.1063/1.4752165

[13] D. Schmid, M. Ruckh, F. Grunwald, H.W. Schock, Chalcopyrite/defect chalcopyrite heterojunctions on the basis of $CuInSe_2$, J. Appl. Phys. 73 (1993) 2902–2909. https://doi.org/10.1063/1.353020

[14] T. Nishimura, Y. Hirai, Y. Kurokawa, A. Yamada, Control of valence band offset at CdS/$Cu(In,Ga)Se_2$ interface by inserting wide-bandgap materials for suppression of interfacial recombination in $Cu(In,Ga)Se_2$ solar cells, Jpn. J. Appl. Phys. 54 (2015) 08KC08. https://doi.org/10.7567/JJAP.54.08KC08

[15] T. Maeda, W. Gong, T. Wada, $CuInSe_2$, $CuIn_3Se_5$, and $CuIn_5Se_8$ phases in Cu-poor Cu_2Se–In_2Se_3 pseudo-binary system – Their crystal structures, optical properties and electronic structures, Current Opinion in Green and Sustainable Chemistry 4 (2017) 77–83. https://doi.org/10.1016/j.cogsc.2017.03.004

[16] C. Insignares-Cuello, C. Broussillou, V. Bermúdez, E. Saucedo, A. Pérez-Rodríguez, V. Izquierdo-Roca, Raman scattering analysis of electrodeposited $Cu(In,Ga)Se_2$ solar cells: Impact of ordered vacancy compounds on cell efficiency, Appl. Phys. Lett. 105 (2014) 021905. https://doi.org/10.1063/1.4890970

[17] A. Coelho, J. Evans, I. Evans, A. Kern, S. Parsons, The TOPAS symbolic computation system, Powder Diffr. 26 (2011) S22–S25. https://doi.org/10.1154/1.3661087

[18] TOPAS, v6.0 (Computer Software), Bruker AXS, Karslruhe, Germany, 2011.

[19] R. Cheary, A. Coelho, J. Cline, Fundamental parameters line profile fitting in laboratory diffractometers, J. Res. Natl. Inst. Stan. 109 (2004) 1–25. https://dx.doi.org/10.6028%2Fjres.109.002

[20] Davor Balzar, X-Ray diffraction line broadening: modeling and applications to high-tc superconductors, J. Res. Natl. Inst. Stan. 98 (1993) 321–353. https://dx.doi.org/10.6028%2Fjres.098.026

[21] P. Jackson, R. Wuerz, D. Hariskos, E. Lotter, W. Witte, M. Powalla, Effects of heavy alkali elements in $Cu(In,Ga)Se_2$ solar cells with efficiencies up to 22.6%, Phys. Status Solidi RRL 10 (2016) 583–586. https://dx.doi.org/10.1002/pssr.201600199

[22] H. Tanino, T. Maeda, H. Fujikake, H. Nakanishi, S. Endo, T. Irie, Raman spectra of $CuInSe_2$, Phys. Rev. B 45 (1992) 13323–13330.

[23] Chuan-Ming Xu, Xiao-Liang Xu, Jun Xu, Xiao-Jie Yang, Jian Zuo, Ning Kong, Wen-Hao Huang, Hong-Tu Liu, Composition dependence of the Raman A_1 mode and additional mode in tetragonal Cu–In–Se thin films, Semicond. Sci. Technol. 19 (2004) 1201–1206. https://doi.org/10.1088/0268-1242/19/10/006

[24] Paul Pistor, Alejandro Ruiz, Andreu Cabot, Victor Izquierdo-Roca, Advanced Raman spectroscopy of methylammonium lead iodide: development of a non-destructive characterisation methodology, Sci. Rep. 6 (2016) 35973. https://doi.org/10.1038/srep35973

[25] Stener Lie, Shin Woei Leow, Douglas M. Bishop, Maxim Guc, Victor Izquierdo-Roca, Oki Gunawan, Lydia Helena Wong, Improving carrier-transport properties of CZTS by Mg incorporation with spray pyrolysis, ACS Appl. Mater. Inter. 11 (2019) 25824–25832. https://doi.org/10.1021/acsami.9b05244

[26] Thomas Feurer, Romain Carron, Galo Torres Sevilla, Fan Fu, Stefano Pisoni, Yaroslav E. Romanyuk, Stephan Buecheler, Ayodhya N. Tiwari, Efficiency improvement of near-stoichiometric $CuInSe_2$ solar cells for application in tandem devices, Adv. Energy Mater. 9 (2019) 1901428. https://doi.org/10.1002/aenm.201901428

[27] Philip Jackson, Dimitrios Hariskos, Roland Wuerz, Wiltraud Wischmann, Michael Powalla, Compositional investigation of potassium doped $Cu(In,Ga)Se_2$ solar cells with efficiencies up to 20.8%, Phys. Stat. Solidi RRL 8 (2014) 219–222. https://doi.org/10.1002/pssr.201409040

[28] B. Minceva-Sukarova, M. Najdoski, I. Grozdanov, C.J. Chunnilall, Raman spectra of thin solid films of some metal sulfides, J. Mol. Struct. 410-411 (1997) 267–270. https://doi.org/10.1016/S0022-2860(96)09713-X

[29] M. Ishii, K. Shibata, H. Nozaki, Anions distributions and phase transitions in $CuS_{1-x}Se_x$ (x = 0-1) studied by Raman spectroscopy, J. Solid State Chem. 105 (1993) 504–511. https://doi.org/10.1006/jssc.1993.1242

[30] C. Xue, D. Papadimitriou, Y. S. Raptis, W. Richter, N. Esser, S. Siebentritt, M. Ch. Lux-Steiner, Micro-Raman study of orientation effects of Cu_xSe-crystallites on Cu-rich $CuGaSe_2$ thin films, J. Appl. Phys. 96 (2004) 1963–1966. https://doi.org/10.1063/1.1772885

[31] K. Kambas, C. Julien, M. Jouanne, A. Likforman, M. Guittard, Raman spectra of α- and γ-In_2Se_3, Phys. Stat. Sol. B 124 (1984) K105–K108. https://doi.org/10.1002/pssb.2221240241

[32] R. Lewandowska, R. Bacewicz, J. Filipowicz, W. Paszkowicz, Raman scattering in α-In_2Se_3 crystals, Mater. Res. Bull. 36 (2001) 2577–2583. https://doi.org/10.1016/S0025-5408(01)00746-2

[33] J. Weszka, Ph. Daniel, A. Burian, A.M. Burian, A.T. Nguyen, Raman scattering in In_2Se_3 and $InSe_2$ amorphous films, J. Non-Cryst. Solid 265 (2000) 98–104. https://doi.org/10.1016/S0022-3093(99)00710-3

[34] C. H. de Groot, J.S. Moodera, Growth and characterization of a novel In_2Se_3 structure, J. Appl. Phys. 89 (2001) 4336–4340. https://doi.org/10.1063/1.1355287

[35] O.A. Balitskii, V.P. Savchyn, V.O. Yukhymchuk, Raman investigation of InSe and GaSe single-crystals oxidation, Semicond. Sci. Technol. 17 (2002) L1-L4. https://doi.org/10.1088/0268-1242/17/2/101

[36] Vladimir V. Poborchii, Alexander V. Kolobov, Kazunobu Tanaka, An in situ Raman study of polarization-dependent photocrystallization in amorphous selenium films, Appl. Phys. Lett. 72 (1998) 1167. https://doi.org/10.1063/1.121002

[37] J Łazewski, K Parlinski, B Hennion, R Fouret, First-principles calculations of the lattice dynamics of $CuInSe_2$, J. Phys.: Condens. Matter 11 (1999) 9665–9671. https://doi.org/10.1088/0953-8984/11/48/323

[38] C. Rincon, F.J. Ramirez, Lattice vibrations of $CuInSe_2$ and $CuGaSe_2$ by Raman microspectrometry, J. Appl. Phys.72 (1992) 4321. https://doi.org/10.1063/1.352195

[39] J. M. Merino, J. L. Martin de Vidales, S. Mahanty, R. Diaz, F. Rueda, M. Leon, Composition effects on the crystal structure of $CuInSe_2$, J. Appl. Phys. 80 (1996) 5610–5616. https://doi.org/10.1063/1.363611

[40] Christiane Stephan, Susan Schorr, Michael Tovar, Hans-Werner Schock, Comprehensive insights into point defect and defect cluster formation in $CuInSe_2$, Appl. Phys. Lett. 98 (2011) 091906. https://doi.org/10.1063/1.3559621

[41] H.M. Rietveld, A profile refinement method for nuclear and magnetic structures, J. Appl. Cryst. 2 (1969) 65–71. https://doi.org/10.1107/S0021889869006558

[42] Koji Takei, Tsuyoshi Maeda, Feng Gao, Seiji Yamazoe, Takahiro Wada, Off-stoichiometric semiconductors $Cu_{1.33+x}Zn_{1.33-x}In_{1.33}Se_4$ (x = 0, 0.1, 0.2 and 0.3): Synthesis, structure, and thermal and electrical properties, Jpn. J. Appl. Phys. 53 (2014) 05FW07-1. https://doi.org/10.1016/j.jssc.2021.122058

[43] S. Lehmann, D. Fuertes Marron, M. Leon, R. Feyerherm, E. Dudzik, E.J. Friedrich, M. Tovar, Y. Tomm, C. Wolf, S. Schorr, T. Schedel Niedrig, M.C. Lux Steiner, J.M. Merino, Long-range structure of $Cu(In_xGa_{1-x})_3Se_5$: A complementary neutron and anomalous X-ray diffraction study, J. Appl. Phys. 109 (2011) 013518. https://doi.org/10.1063/1.3524183

[44] K. Momma, F. Izumi, VESTA 3 for three-dimensional visualization of crystal, volumetric and morphology data, J. Appl. Crystallogr. 44 (2011) 1272–1276. https://doi.org/10.1107/S0021889811038970

[45] S.B. Zhang, Su-Huai Wei, Alex Zunger, Defect physics of the $CuInSe_2$ chalcopyrite semiconductor, Phys. Rev. B 57 (1998) 9642-9656. https://doi.org/10.1103/PhysRevB.57.9642

[46] Lauryn L. Baranowski, Pawel Zawadzki, Steven Christensen, Dennis Nordlund, Stephan Lany, Adele C. Tamboli, Lynn Gedvilas, David S. Ginley, William Tumas, Eric S. Toberer, Andriy Zakutayev, Control of doping in Cu_2SnS_3 through defects and alloying, Chem. Mater. 26 (2014) 4951–4959. https://doi.org/10.1021/cm501339v

[47] Mirjana Dimitrievska, Andrew Fairbrother, Edgardo Saucedo, Alejandro Pérez-Rodríguez, Victor Izquierdo-Roca, Influence of compositionally induced defects on the vibrational properties of device grade $Cu_2ZnSnSe_4$ absorbers for kesterite based solar cells, Appl. Phys. Lett. 106 (2015) 073903. https://doi.org/10.1063/1.4913262

[48] Mirjana Dimitrievska, Florian Oliva, Maxim Guc, Sergio Giraldo, Edgardo Saucedo, Alejandro Pérez-Rodríguez, Victor Izquierdo-Roca, Defect characterisation in $Cu_2ZnSnSe_4$ kesterites via resonance Raman spectroscopy and the impact on optoelectronic solar cell properties, J. Mater. Chem. A 7 (2019) 13293–13304. https://doi.org/10.1039/C9TA03625C

[49] Alex Polizzotti, Ingrid L. Repins, Rommel Noufi, Su-Huai Wei, David B. Mitzi, The state and future prospects of kesterite photovoltaics, Energy Environ. Sci. 6 (2013) 3171–3182. https://doi.org/10.1039/C3EE41781F

[50] Su-Huai Wei, S. B. Zhang, Alex Zunger, Effects of Ga addition to $CuInSe_2$ on its electronic, structural, and defect properties, Appl. Phys. Lett. 72 (1998) 3199. https://doi.org/10.1063/1.121548

[51] C. S. Schnohr, H. Kammer, C. Stephan, S. Schorr, T. Steinbach, J. Rensberg, Atomic-scale structure and band-gap bowing in $Cu(In,Ga)Se_2$, Phys. Rev. B 85 (2012) 245204. https://doi.org/10.1103/PhysRevB.85.245204

[52] Victor Izquierdo-Roca, Xavier Fontané, Edgardo Saucedo, Jesus Salvador Jaime-Ferrer, Jacobo Álvarez-García, Alejandro Pérez-Rodríguez, Veronica Bermudez, Joan Ramon Morante, Process monitoring of chalcopyrite photovoltaic technologies by Raman spectroscopy: an application to low cost electrodeposition based processes, New J. Chem. 35 (2011) 453–460. https://doi.org/10.1039/C0NJ00794C

[53] R. Herberholz, U. Rau, H.W. Schock, T. Haalboom, T. Gödecke, F. Ernst, C. Beilharz, K.W. Benz, D. Cahen, Phase segregation, Cu migration and junction formation in $Cu(In,Ga)Se_2$, Eur. Phys. J. AP 6 (1999) 131–139. https://doi.org/10.1051/epjap:1999162

[54] Dongxiang Liao, Angus Rockett, Cu depletion at the $CuInSe_2$ surface, Appl. Phys. Lett. 82 (2003) 2829. https://doi.org/10.1063/1.1570516

[55] H. Mönig, Ch.-H. Fischer, A. Grimm, B. Johnson, C. A. Kaufmann, R. Caballero, I. Lauermann, M. Ch. Lux-Steiner, Surface Cu-depletion of $Cu(In,Ga)Se_2$ thin films: Further experimental evidence for a defect-induced surface reconstruction, J. Appl. Phys. 107 (2010) 113540. https://doi.org/10.1063/1.3427539

[56] P. Pistor, D. Greiner, C.A. Kaufmann, S. Brunken, M. Gorgoi, A. Steigert, W. Calvet, I. Lauermann, R. Klenk, T. Unold, M.-C. Lux-Steiner, Experimental indication for band gap widening of chalcopyrite solar cell absorbers after potassium fluoride treatment, Appl. Phys. Lett. 105 (2014) 063901. https://doi.org/10.1063/1.4892882

[57] Tim Kodalle, Tobias Bertram, Rutger Schlatmann, Christian A. Kaufmann, Effectiveness of an RbF post deposition treatment of CIGS solar cells in dependence on the Cu content of the absorber layer, IEEE J. Photovoltaics 9 (2019) 1839–1845. https://doi.org/10.1109/JPHOTOV.2019.2929418